nature sustainability

Article

https://doi.org/10.1038/s41893-023-01233-2

Solar-driven waste-to-chemical conversion by wastewater-derived semiconductor biohybrids

Received: 28 February 2023

Accepted: 15 September 2023

Published online: 16 October 2023

Check for updates

Shanshan Pi[1,2,6], Wenjun Yang[2,6], Wei Feng[3,6], Ruijie Yang[1], Weixiang Chao[1], Wenbo Cheng[4], Lei Cui[2], Zhida Li[1], Yiliang Lin[5], Nanqi Ren[1], Chen Yang[4], Lu Lu[1] ✉ & Xiang Gao[2] ✉

Semiconductor biohybrids integrating the merits of living cells and semiconductor materials have the potential to shift the current energy-intensive chemical production system to a more sustainable one by offering efficient solar-to-chemical conversion. However, cost-competitive and environmentally friendly scaling-up approaches are still urgently needed. To tackle this challenge, we propose a strategy that co-utilizes pollutants in wastewater to produce semiconductor biohybrids *in-situ* for scalable solar-to-chemical conversion. Specifically, we introduce an aerobic sulfate reduction pathway into *Vibrio natriegens* to enable the direct utilization of heavy metal ions (that is, Cd^{2+}), sulfate and organics in wastewater to biosynthesize functional semiconductor nanoparticles in living *V. natriegens* to assemble semiconductor biohybrids. Meanwhile, a designated biosynthetic pathway is introduced into the biohybrids to enable the production of 2,3-butanediol, a valuable bulk chemical with wide applications, from organics in wastewater. Using the obtained biohybrids, the production of 2,3-butanediol reaches 13.09 g l^{-1} in a 5-l illuminated fermenter using wastewater as the feedstock, revealing its scalability. Life-cycle assessment shows that this specific biohybrid route has substantial sustainability gain compared with conventional 2,3-butanediol production routes. This work can bring solar-driven biomanufacturing and waste-to-wealth conversion one step forward and pave the way to cleaner production and circular economy.

Current industrial chemicals are primarily derived from fossil fuels, resulting in excessive carbon emissions and climate change and raising sustainability concerns. There is a clear need for the environmentally sustainable, affordable manufacturing of chemicals[1,2]. Biomanufacturing with sugar fermentation offers an opportunity to switch from fossil fuels to renewable energy sources, which contributes a more sustainable production of chemicals (Fig. 1a)[1,3]. However, in conventional biomanufacturing, the sugar substrates undergo oxidation to generate reducing energy (NAD(P)H), which releases CO_2 and reduces carbon yields during chemical production[1,4]. This is where semiconductor biohybrids stand out recently[5,6]. By integrating efficient light-harvesting materials with microbial cell factories, the biohybrids promise an avenue where solar energy can be directly channelled into chemical production, thereby reducing/eliminating carbon loss (Fig. 1a,b)[5–7]. Currently, there are limited applications of semiconductor hybrids due to the relatively high cost associated with large-scale biohybrid

A full list of affiliations appears at the end of the paper. ✉e-mail: lulu@hit.edu.cn; gaoxiang@siat.ac.cn

construction[8,9]. On one hand, traditional semiconductor synthesis through physical or chemical methods is uneconomical and environmentally unsustainable[10]. On the other hand, biosynthesis of semiconductor nanoparticles, such as cadmium sulfide, via microorganisms typically involves a costly cysteine precursor[5,11,12]. It remains a major challenge to leverage biohybrids to achieve scalable chemical production in a cost-effective and environmentally sustainable manner.

The waste-to-wealth approach is well aligned with renewable energy and eco-friendly sustainability[13,14]. In recent years, sustainable biomanufacturing has exhibited the potential to produce a range of commodity chemicals from waste, including plastics[15], food waste[16] and industrial gases[2]. Recently, an engineered sulfide-producing yeast was constructed to precipitate heavy metals in sulfate-amended wastewater by forming metal sulfide as potential semiconductor for environmental remediation[17]. Thus, it is a promising approach to directly use wastewater containing sulfate, heavy metals and organic pollutants as feedstock towards biohybrid synthesis for solar-to-chemical production, turning the waste into wealth. However, real industrial wastewater usually varies in major organics[18,19], heavy metals[20,21] and complex pollutants (details in compositions of industrial wastewater are provided in Methods). It also contains high salt[22,23] and dissolved oxygen that requires an aerobic sulfate reduction ability in microbial hosts[24]. In contrast, conventional sulfate reduction using wild-type microbes is an anaerobic process[25]. Thus, there remain challenges associated with biohybrid synthesis for biomanufacturing using wastewater.

Here we design and engineer *Vibrio natriegens* to synthesize semiconductor biohybrids directly from real industrial wastewater and further produce a commodity chemical at a 5-l scale (Fig. 1c). *Vibrio natriegens*, a marine bacterium, is a promising industrial production host with fast growth rate (doubling time <10 min), high substrate consumption rates[26], exceptional tolerance to high salt concentration and capability of utilizing various carbon sources, including most carbohydrates, proteins, carboxylic/aromatic acids and alcohols[18]. Thus, *V. natriegens* could be a great candidate to utilize wastewater for solar-to-chemical production via turning waste into wealth. An aerobic sulfate reduction pathway was engineered into *V. natriegens*, and the resulting strain could produce hydrogen sulfide (H_2S) directly from sulfate in industrial wastewater and further biomineralize the metal ions to form biohybrids *in-situ*. This was confirmed by electron microscopy imaging, X-ray diffraction (XRD) and inductively coupled plasma mass spectrometry (ICP–MS). We further introduced a 2,3-butanediol (BDO) biosynthetic pathway to enable the biohybrids to produce BDO from organics in wastewater. The resulting biohybrid cells increased intracellular reduced nicotinamide adenine dinucleotide (NADH) under light condition and facilitated higher BDO production and higher conversion yield compared with pure bacterial cells (Fig. 1c).

A 5-l scale fed-batch fermentation using real industrial wastewater was conducted to show the potential of *in-situ* engineered biohybrid construction and scalable solar-driven BDO production from multiple pollutants. Life-cycle assessment (LCA) confirmed that the wastewater-based biohybrid platform has lower greenhouse gas (GHG) emission, product cost and comprehensive environmental impacts, when compared with both pure bacterial fermentation and fossil-based routes for BDO production (Fig. 1b). By developing a cost-competitive and environmentally friendly approach for the sustainable production of semiconductor biohybrids towards solar-driven chemical production utilizing abundant wastes in wastewater, we provide a potential bridge between fundamental research of biohybrids and their practical applications.

Results

Engineering microbes to assemble semiconductor biohybrids

The organics, heavy metal ions and sulfate in wastewater can serve as major substrates for semiconductor biohybrid construction and solar-to-chemicals production (Fig. 1c). To achieve biohybrid construction in wastewater and waste-to-wealth sustainability, our first step was to engineer *V. natriegens* so that it produced sulfide directly from sulfate, a common pollutant in wastewater[27], rather than adding expensive cysteine precursors. The conversion of sulfate to H_2S occurs in nature via a diverse group of sulfate-reducing bacteria (SRB), but these bacteria have a slow growth rate and typically require strict cultivation conditions because they are obligate anaerobes[25]. Moreover, SRB usually metabolize simple organics to reduce sulfate[20,25]. Alternatively, an aerobic sulfate reduction pathway was engineered in *E. coli* by introducing two unique enzymes: (1) a serine acetyltransferase (CysE) directing native assimilatory sulfate reduction to overproduce cysteine and (2) *cdsH* encoding cysteine desulfhydrase (CdsH) converting excess cysteine to H_2S[24]. Inspired by this, we introduced a pathway containing a mutant CysE that is insensitive to feedback inhibition by cysteine and CdsH into *V. natriegens* (Fig. 2a), resulting in an aerobic strain of XG203. To examine the capability to produce H_2S, we cultured strain XG203 in a well-defined minimum medium (MM) with sulfate supply. Strain XG203 produced 106 ppm H_2S in 24 h and the average production rate reached ~4.42 ppm h^{-1} (Fig. 2b). Meanwhile, there was no detectable H_2S produced in wild-type (WT) *V. natriegens* even after 24 h (Fig. 2c), confirming the successful introduction of the aerobic sulfide production pathway.

We further cultured strain XG203 in well-defined MM with sulfate and 0.1 mM $CdCl_2$ to investigate its capability to utilize the heavy metal resources with the production of H_2S. Impressively, almost all the Cd^{2+} (99.91%) were removed within ~2 h, with a removal rate of 4.56 mg l^{-1} h^{-1} (Supplementary Fig. 1a). The bacterial culture simultaneously became yellow, suggesting the formation of CdS nanoparticles (Fig. 2b). Meanwhile, theWT *V. natriegens* remained white in colour and only removed 1.19% Cd^{2+} from the medium even after 24 h (Fig. 2c). There was no nanoparticle observed on the WT cells (Supplementary Fig. 2) and multiple benchmark experiments confirmed that this small portion of Cd^{2+} was absorbed by various metal-binding groups on the cell wall as reported previously[21].

To confirm that the yellow pellets were CdS–bacteria hybrids, we first visualized them using electron microscopy. Scanning electron microscope (SEM) images showed that bacterial cells in the hybrids deposit nanoparticles with an average size of ~55.11 nm *in-situ* (Fig. 2d and Supplementary Fig. 1b), while there were no obvious nanoparticles observed in *V. natriegens* cultured in medium without Cd^{2+} (Supplementary Fig. 1c). Energy dispersive spectroscopy (EDS) mapping confirmed that these particles are composed of Cd and S elements (Fig. 2d). Furthermore, we prepared cross-sectional samples through microtoming. Scanning transmission electron microscopy energy dispersive spectroscopy (STEM-EDS) mapping showed that the particles are also composed of Cd and S elements (Fig. 2e,f). We speculate that the intracellularly produced H_2S, a high-membrane-permeability gas[28], readily diffused to the cell surface where it reacted with Cd^{2+} to form CdS nanoparticles (CdS NPs). Therefore, the CdS NPs were mainly distributed on the cell surface of the engineered strain (Fig. 2e and Supplementary Fig. 1f,g), similar to other microorganisms[5,17].

Afterwards, we lysed the biohybrids and collected the nanoparticles for further characterization. The nanoparticles have a good crystallinity with main lattice spacing of 3.36 Å and 2.05 Å (Supplementary Fig. 1d,e), and XRD patterns confirmed that these nanoparticles are CdS (Supplementary Fig. 1h). High-resolution X-ray photoelectron spectroscopy (XPS) of Cd 3d also confirmed that the chemical state of the cadmium species is Cd (II) in the nanoparticles (Supplementary Fig. 1i). STEM analysis revealed that these dispersive nanoparticles have an average size of ~5.54 nm, which is similar to previous reports of extracted nanoparticles in microorganisms[10,29] (Fig. 2g). Notably, the size of lysed particles is much smaller than the particles deposited on the cell surfaces, indicating aggregation of multiple particles (~10) during biosynthesis. High-angle annular dark-field STEM (HAADF–STEM) and selected area electron diffraction (SAED) of the particles indicated

https://doi.org/10.1038/s41893-023-01233-2

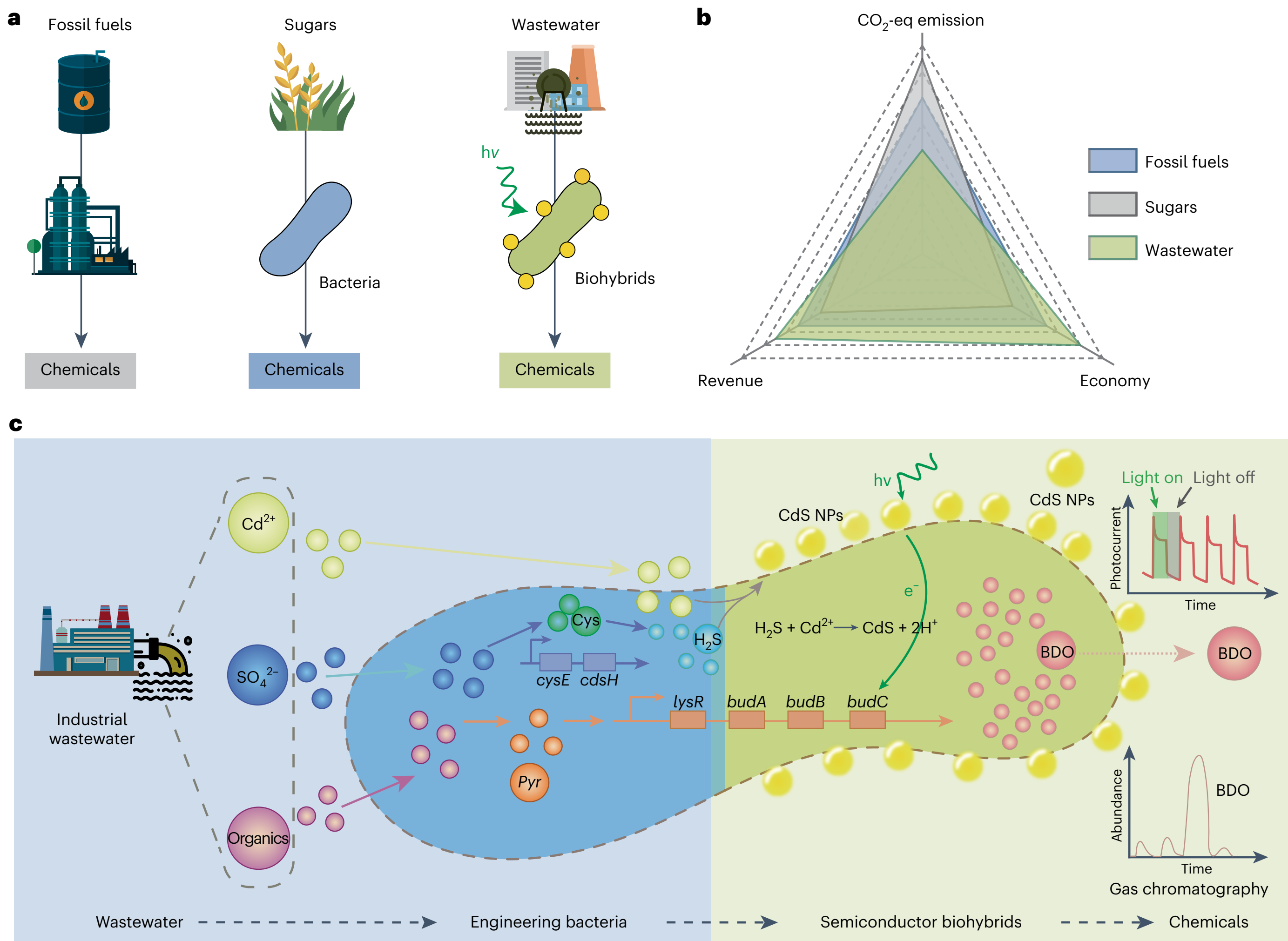

Fig. 1 | Schematic of solar-driven chemical production by semiconductor biohybrids synthesized from wastewater pollutants using engineered *V. natriegens*. **a**, Schematic of chemical production by refinery of fossil fuels, sugar fermentation and biohybrids using wastewater. **b**, Comprehensive evaluation of sustainability of these routes by CO_2 equivalent of GHG emissions, economy of cost advantages and revenue from extended by-products and environmental remediation. **c**, The industrial wastewater usually contains multipollutants including Cd^{2+}, sulfate and organics. These pollutants could be co-utilized by engineered *V. natriegens* to construct a biohybrid system for solar-driven chemical production *in-situ*.

a polycrystalline structure (Fig. 2g and Supplementary Fig. 1d). To discern the function of the biomineralized CdS NPs, we performed UV–Vis spectrum and electrochemical characterization to measure photoelectrochemical performance of particles. The CdS NPs have a direct band energy of ~2.58 eV with a conduction band of about −0.78 eV (Supplementary Fig. 1j,k), and the photo-induced current was ~0.53 μA cm^{-2} (Fig. 2h), which is close to the range in previous reports[12,30].

The concentrations of heavy metal ions, such as Cd^{2+}, in common industrial wastewater have a wide range from several ppm to thousands of ppm[31–33]. For high-concentration wastewater, a pretreatment-based chemical/physical (for example, precipitation and adsorption) approach is generally set within factories by mandatory regulations to remove most metals and reduce environmental risks[34]; this leads to an effluent with relative low metal ion concentration (below dozens of ppm) that is compatible with sustainable biological treatment[31,35], such as that in domestic wastewater treatment plants. To confirm the capability of strain XG203 to form biohybrids from the majority of wastewater resources, we cultured strain XG203 with Cd^{2+} from 0.01 mM to 0.2 mM (1–22 ppm) as a stress testing. Surprisingly, the engineered strain removed almost all the Cd^{2+} (above 99%) when the concentration was not more than 0.15 mM and removed 81.92% of Cd^{2+} with negligible inhibition of bacterial growth even in a very high concentration (0.2 mM Cd^{2+}) (Fig. 2i). Also, with the increase in Cd^{2+} concentration in the medium, the culture became more yellow, which is consistent with the increase in biohybrids and CdS nanoparticle formation (Fig. 2i). This strategy can be extended to other heavy metals such as Pb^{2+} (~0.3 mM) and Hg^{2+} (~0.025 mM), and heavy metal-contaminated wastewaters are feedstocks for hybrid construction with benefits of effective remediation (Supplementary Fig. 3 and Table 2). The universality of our developed strategy was further demonstrated by other metallic sulfides, such as PbS (Supplementary Fig. 4) and HgS (Supplementary Fig. 5).

Engineering microbes to utilize organics in wastewater

Aside from the different species and concentrations of heavy metal ions in industrial wastewater, organics can also vary substantially[18,19]. To establish a sustainable and economical chemical production process, strain XG203 needs to be able to adapt to different organics in wastewater resources. The major organic component in different industrial wastewater varies. For instance, wastewater generated during sugar production mainly includes molasses, while that generated in biodiesel production generally contains glycerol[36,37]. Molasses waste is a complex of sucrose, fructose and glucose according to high-performance liquid chromatography (HPLC) analysis (Supplementary Table 3). To test the

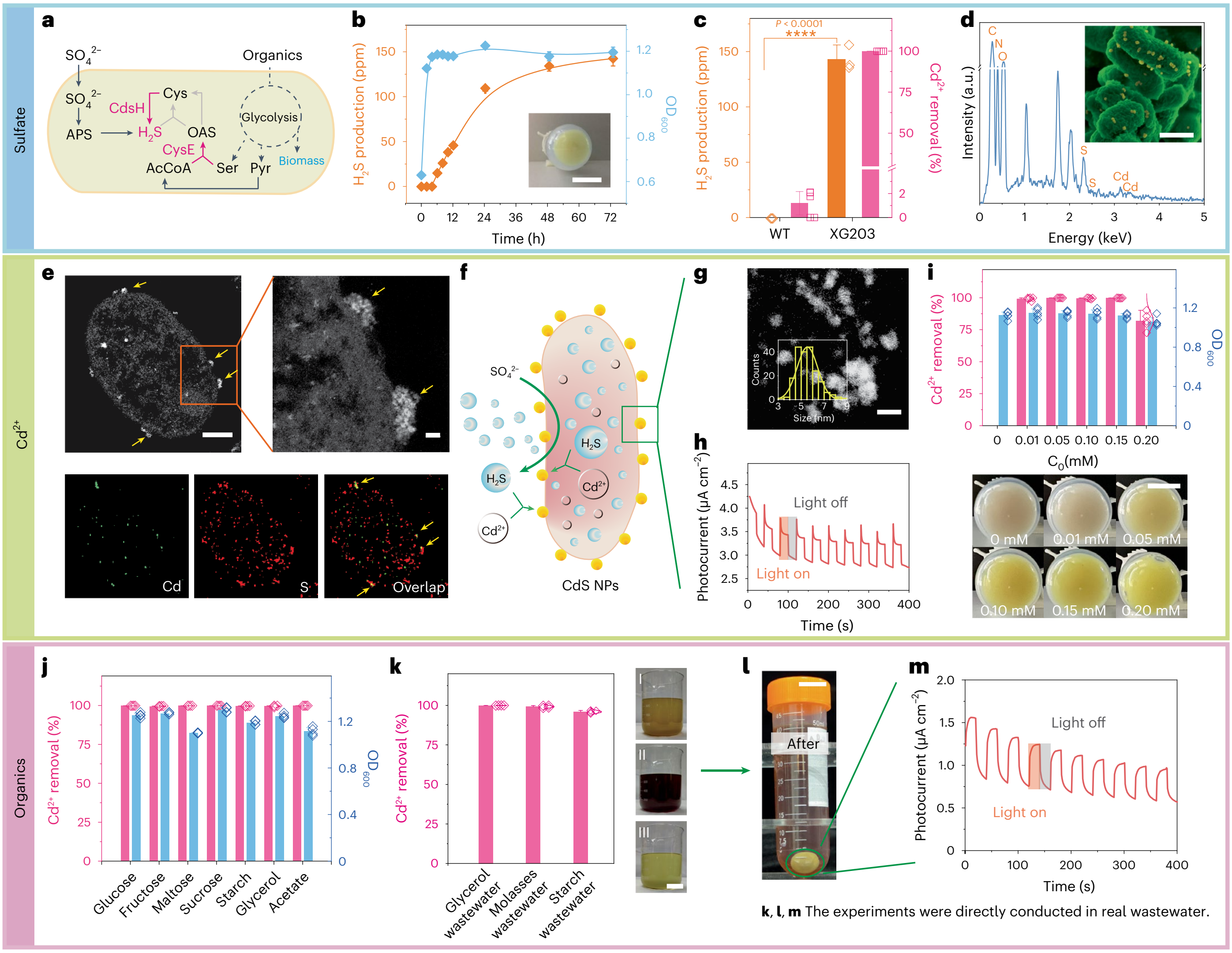

Fig. 2 | Designing *V. natriegens* to produce semiconductor biohybrids from wastewater. **a**, Overexpressed CysE and CdsH in *V. natriegens* to produce H_2S from SO_4^{2-}. OAS, *O*-acetylserine; Pyr, pyruvate; Ser, serine; AcCoA, acetyl-CoA; APS, adenosine 5′-phosphosulfate; Cys, cysteine. **b**, H_2S production and cell growth of strain XG203 in well-defined MM. Data are presented as mean ± s.d. ($n = 3$, biologically independent samples). Inset: pellet of strain XG203 after culturing with Cd^{2+}. Scale bar, 2 cm. **c**, Cd^{2+} removal and H_2S production between wild-type and engineered *V. natriegens*. Data are presented as mean ± s.d. ($n = 3$ for H_2S production; $n = 5$ for Cd^{2+} removal). **d**, SEM image (inset) and EDS mapping of biohybrid sample collected from **c**. Green structures and yellow dots represent bacterial cells and nanoparticles in biohybrids, respectively. Scale bar, 0.5 μm. **e**, Cross-sectional STEM image of biohybrid sample collected from **c**. Bottom, the STEM-EDS mapping images. Yellow arrows, CdS nanoparticles. Scale bars, 0.2 μm (left) and 20 nm (right). **f**, Schematic of semiconductor biohybrid construction. **g**, HAADF–STEM image of isolated CdS NPs. High-resolution TEM (HRTEM) images were used to analyse the size of nanoparticles (more than 200 particles). Scale bar, 5 nm. **h**, A representative photocurrent curve of isolated nanoparticles lysed from biohybrids of **c**. **i**, Top: the strain XG203 was cultured with sulfate and different concentrations of Cd^{2+} (0.01–0.2 mM) for biohybrid construction. Bottom: corresponding pellets. Data are presented as mean ± s.d. ($n = 5$). Scale bar, 1.5 cm. **j**, Cd^{2+} removal and cell growth of strain XG203 after culturing in well-defined MM with common carbon sources from wastewater. Data are presented as mean ± s.d. ($n = 4$). **k**, Left: Cd^{2+} removal of strain XG203 using three kinds of real wastewater, with glycerol wastewater (I), molasses wastewater (II) and starch wastewater (III) as carbon sources, respectively. Right: visual representation of corresponding wastewaters. Data are presented as mean ± s.d. ($n = 4$). Scale bar, 5 cm. **l**, The pellets of engineered strain after culturing in molasses wastewater collected from **k**. Scale bar, 1.5 cm. **m**, A representative photocurrent curve of biohybrid samples collected from **l**. All *P* values were determined using a two-tailed unpaired *t*-test.

broad spectrum of substrate utilization, we cultured strain XG203 in well-defined MM (amendment with sulfate and Cd^{2+}) with different organics, including glucose, fructose, maltose, sucrose, starch, glycerol and acetate. We found that strain XG203 could grow very well with different organics, with high Cd^{2+} (all above 99%) removal efficiency and biohybrid formation (Fig. 2j and Supplementary Fig. 1l).

We further utilized real industrial wastewater (detailed composition in Supplementary Table 4), which was prepared by mixing organic wastewater (generated by biodiesel, corn starch or sugar industries, with detailed compositions in Supplementary Table 3) with electroplating wastewater (detailed composition in Supplementary Table 5). The strain could synthesize biohybrids and simultaneously achieve high Cd^{2+} removal efficiency of 95.93–99.92% (Fig. 2k). The bacterial culture turned yellow over time, indicating the generation of CdS biohybrids using wastewater (Fig. 2l). We further collected the biohybrids directly synthesized from real industrial wastewater with organics supplied by molasses wastewater for photoelectrochemical measurement, and the biohybrids show a photo-induced current of ~0.51 μA cm^{-2} (Fig. 2m), which is close to the photocurrent of previously reported biohybrids[38] and slightly lower than that of isolated CdS

 https://doi.org/10.1038/s41893-023-01233-2

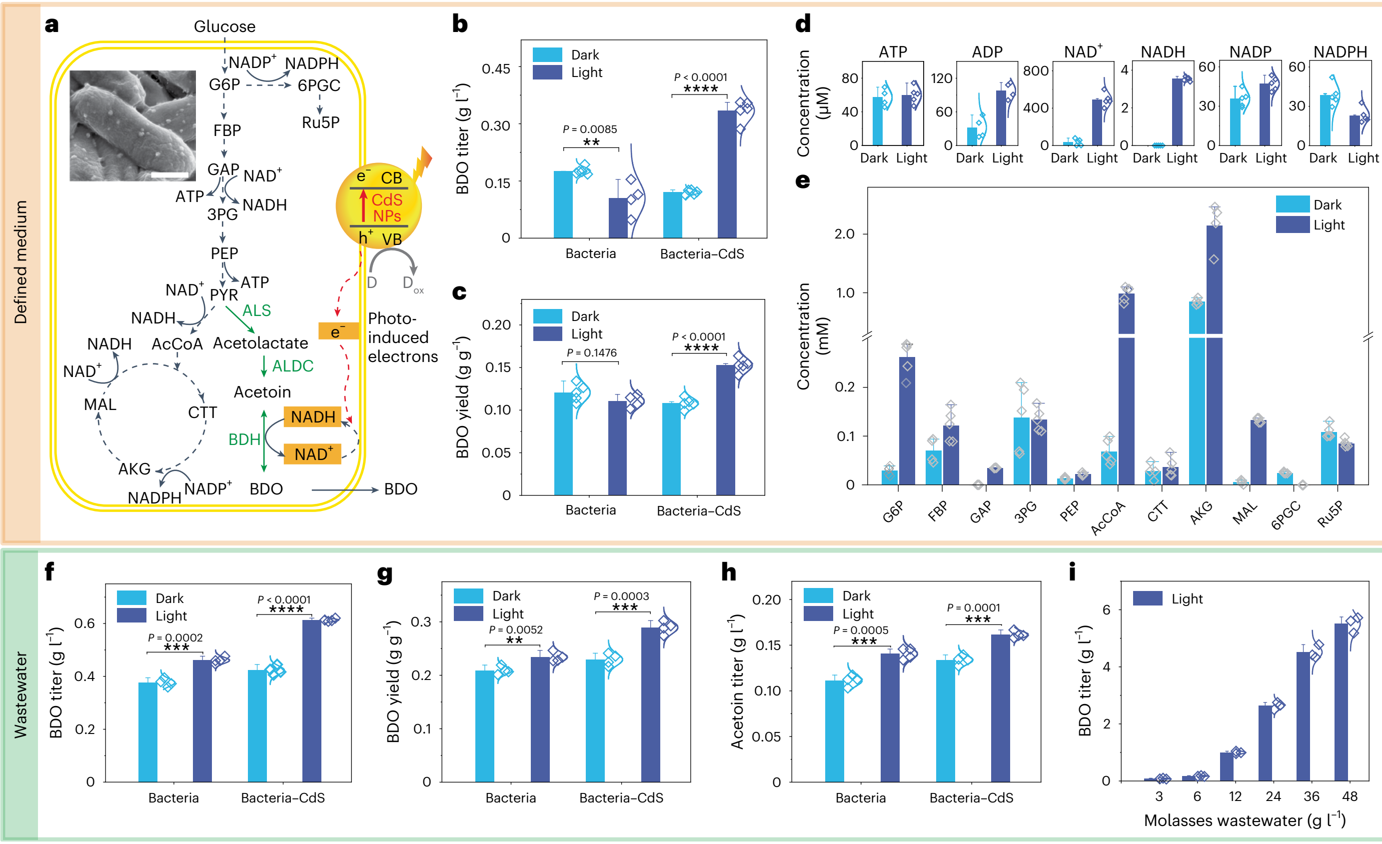

Fig. 3 | Solar-to-chemical production by the semiconductor biohybrids from wastewater. a, A solar-enhanced BDO biosynthetic pathway in semiconductor biohybrids. G6P, glucose 6-phosphate; FBP, fructose 1,6-bisphosphate; GAP, glyceraldehyde 3-phosphate; 3PG, 3-phosphoglycerate; PEP, phosphoenolpyruvate; CTT, citrate; AKG, α-ketoglutarate; MAL, malate; 6PGC, 6-phosphogluconate; Ru5P, ribulose 5-phosphate; CdS NPs, CdS nanoparticles; CB, conduction band; VB, valence band; D, electron donor; D_{ox}, oxidized donor. Green text and arrows, the enzymes and reactions of BDO biosynthetic pathway. Inset: SEM image of semiconductor biohybrids. Scale bar, 0.5 µm. **b**, BDO production by pure bacterial system and bacteria–CdS hybrid system under dark and light conditions. Data are presented as mean ± s.d. (n = 5, 4, 5 and 5, respectively, from left to right). **c**, Glucose-to-BDO conversion yield of bacteria and bacteria–CdS hybrid. Data are presented as mean ± s.d. (n = 5, 4, 5 and 5, respectively, from left to right). **d**, Concentration of intracellular cofactors in biohybrids under dark and light conditions. Data are presented as mean ± s.d. (n = 4 for ADP and ATP under dark and ADP under light, n = 5 for others). **e**, Concentration of intracellular metabolites of central carbon metabolism in biohybrids under dark and light conditions. Data are presented as mean ± s.d. (n = 4 for FBP, CTT, AKG, MAL and 6PGC under dark and AKG under light; n = 5 for others). **f**, BDO production of pure bacterial system and biohybrid system using wastewater under dark and visible-light conditions. Data are presented as mean ± s.d. (n = 4). **g**, Waste sugar-to-BDO conversion yield of bacterial and biohybrid system using wastewater. Data are presented as mean ± s.d. (n = 4). **h**, Acetoin production of bacterial and biohybrid system using wastewater under dark and visible-light conditions. Data are presented as mean ± s.d. (n = 4). **i**, Solar-driven BDO production by biohybrid system using wastewater containing different concentrations of molasses (3–48 g l^{-1}). Data are presented as mean ± s.d. (n = 3). Light intensity was 4.2 mW cm^{-2} for all experiments under light condition. All P values were determined using a two-tailed unpaired t-test.

nanoparticles. However, the values might not be directly comparable as the number of nanoparticles and interfaces with electrodes are very different between isolated nanoparticles and biohybrids[30].

Taken together, with our tailored and engineered strain, we are able to synthesize semiconductor biohybrids directly from wastewater with successful utilization of the heavy metals, sulfate and organics in wastewater, paving a promising path for large-scale production for biomanufacturers.

Solar-to-chemical production by biohybrids from wastewater

After confirming the successful synthesis of biohybrids using real wastewater resources, we further tested whether these biohybrids could perform solar-to-chemical production *in-situ* for renewable energy and sustainable biomanufacturing. BDO is a promising bulk chemical for a wide range of uses, such as for the production of synthetic rubber[39]. Microbial BDO production has attracted great attention by providing a more sustainable future[39]. Therefore, we introduced the BDO biosynthetic pathway into *V. natriegens* to demonstrate the capability of our biohybrids for solar-to-chemical production. The BDO biosynthetic pathway contains three enzymes (Fig. 3a). Acetolactate synthase (ALS) and acetolactate decarboxylase (ALDC) convert pyruvate to acetoin, which is catalysed by 2,3-butanediol dehydrogenase (BDH) and converted to BDO by using the reducing power of NADH[39,40] (Fig. 3a). We cloned the BDO biosynthetic gene cluster from *Enterobacter cloacae* and expressed it in strain XG203 under the control of a native promoter[41] and the resulting strain was designated as XG203A.

To test the successful integration of the BDO pathway and explore the biological mechanism, we first tested the ability of strain XG203A for light-driven chemical production in well-defined MM (modified M9 medium with 5 g l^{-1} glucose, Cd^{2+}, sulfate, electron sacrificial agent and mediator). We confirmed that the illuminated biohybrid system can produce BDO with a titer of 0.33 g l^{-1}, showing 1.90-fold improvement compared with the bacterial system (Fig. 3b), and the optimal light intensity was 4.2 mW cm^{-2} (Supplementary Fig. 6) which showed no extra reactive oxygen species (ROS) in the hybrid system (Supplementary Fig. 6c). Also, the glucose-to-BDO conversion yield increased from

 https://doi.org/10.1038/s41893-023-01233-2

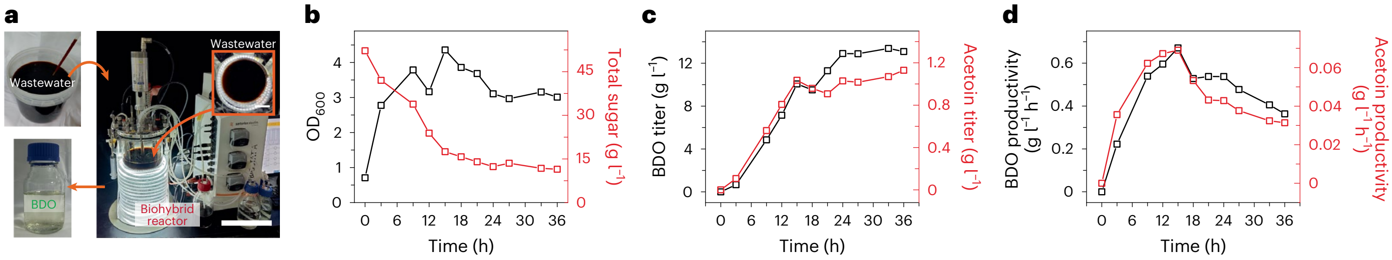

Fig. 4 | Scaling up of chemical production with biohybrid system using real wastewater. a, Visual representation of the 5-l illuminated bioreactor for BDO production by *in-situ* production of semiconductor biohybrids using wastewater. Wastewater is converted to a valuable chemical (BDO) by strain XG203A in the illuminated bioreactor. Scale bars, 20 cm and 6.5 cm (inset). **b**, Time courses of sugar consumption and growth (OD_{600}) of semiconductor biohybrid system during BDO production. **c**, Titers of BDO and acetoin produced by semiconductor biohybrids. **d**, Productivity of BDO and acetoin by semiconductor biohybrids.

0.12 g g^{-1} to 0.15 g g^{-1}, an increase of 26.69% (Fig. 3c), probably due to the regeneration of additional NADH from illuminated CdS nanoparticles (see more discussion below). We also found that the BDO production and yield of the biohybrid system under illumination were respectively 2.78 and 1.41 times those of the dark condition (Fig. 3b,c). However, in the strain XG203A without CdS nanoparticles, the BDO production and yield under light were respectively 40.76% and 8.39% lower than in the dark condition (Fig. 3b,c). The experiment suggests that the biohybrid system could be used for efficient biomanufacturing as previously reported[42–44].

To explore the possible factors contributing to increasing solar-to-chemical production, we collected CdS-biohybrid samples from well-defined MM under light and dark conditions, and performed targeted metabolites quantification using liquid chromatography–tandem mass spectrometry (LC–MS/MS). We first analysed the effect of cofactor regeneration caused by photo-induced electrons[6,9]. We found that NAD^+ and NADH, the major reducing cofactors in heterotrophic microorganisms[45] and are utilized by the BDO synthetic pathway, were respectively increased to 490.58 µM and 3.54 µM in hybrids under light condition, these values being much higher than those under dark condition (Fig. 3d). The outer membrane protein (such as MtrC) may be involved in the photoelectron transfer for the reducing cofactor regeneration (Supplementary Fig. 7). Conversely, NADPH concentration in light condition was 40.41% lower than in the dark, and ATP concentrations were similar under both conditions (Fig. 3d). In bacterial cells, central carbon metabolism is often coupled with energy metabolism[7,46], hence we further analysed the regulation of photo-induced electrons on central carbon metabolism. NADH is mainly produced from the glycolysis pathway (Embden–Meyerhof–Parnas, EMP pathway) and the tricarboxylic acid (TCA) cycle, while NADPH is synthesized from the pentose phosphate pathway (PPP) (Fig. 3a). We found that glucose 6-phosphate (G6P) and fructose 1,6-bisphosphate (FBP) in the EMP pathway and citrate (CTT) and a-ketoglutarate (AKG) in the TCA cycle were increased under light compared with under dark condition (Fig. 3e). Correspondingly, 6-phosphogluconate (6GPC) and ribulose 5-phosphate (Ru5P) in PPP were lower in light condition than in the dark (Fig. 3e). These results suggest that the central carbon metabolism also contributes to the NADH increase in the biohybrid system. In addition, we found that acetoin, a direct precursor for BDO production, increased by 84.33% in light condition (Supplementary Fig. 8a). The higher concentration of substrates, acetoin and NADH, could provide a driving force for BDO production. Taken together, these results suggest that illuminated semiconductor biohybrid systems could stimulate the activity of intracellular metabolism to provide more reducing power and substrates for final chemical production, as also found in previous research[6,46].

After confirming the successful production of BDO with strain XG203A and probing the mechanism behind the photosynthesis, we further applied strain XG203A in real wastewater containing 4.1 g l^{-1} sugar, 0.1 mM Cd^{2+} and 4.02 g l^{-1} sulfate. As shown in Fig. 3f, the BDO production of the illuminated biohybrid system using wastewater was superior to all other conditions, with a titer of 0.61 g l^{-1}, showing 1.45-fold increase compared with its counterpart under dark and 1.33-fold increase compared with engineered bacteria in the absence of nanoparticles under light. Waste organics (sugar)-to-BDO conversion yield also increased 26.10% compared with the dark condition of the biohybrid system (Fig. 3g). Acetoin production using wastewater by the illuminated biohybrid system was also the highest among all other conditions (Fig. 3h and Supplementary Fig. 8b). There was H_2S generated during the BDO production (Supplementary Fig. 9). Moreover, the production of BDO was gradually increased by adding higher concentrations of molasses wastewater in the illuminated biohybrid culture, reaching 5.51 g l^{-1} with 48 g l^{-1} molasses (Fig. 3i). The light-driven BDO production was readily extended to other biohybrid systems (Supplementary Fig. 10), such as bacteria–metal sulfide complexes (with multiple coexisting metals, such as CdS, PbS, CuS and ZnS), which showed even higher BDO production, possibly due to enhanced light absorption and better charge separation under the presence of different semiconductor nanoparticles with various energy levels[47] (Supplementary Figs. 1, 4 and 5). In addition to increased BDO production under illumination, the oxidation–reduction potential of the hybrid system also increased compared with that of the bacterial system (Supplementary Fig. 11), which indicates a light-promoted chemical production using electrons derived from light-activated nanoparticles[48,49]. These experiments suggest that the wastewater-based biohybrid system could be used *in-situ* for efficient solar-to-chemical production, with an increased carbon conversion into chemicals.

Scaling up of chemical production with biohybrids in wastewater

Finally, to demonstrate the performance of biohybrids in scalable chemical production via co-utilization of multiple pollutants in wastewaters, we tested solar-driven BDO production by the *in-situ* production of semiconductor biohybrids using our engineered strain XG203A with a pH-controlled fed-batch 5-l fermenter under illumination (Fig. 4a). XG203A utilized 78.05% of sugars from the wastewater for *in-situ* production of semiconductor biohybrids and chemicals (Fig. 4b). The production of BDO and acetoin reached 13.09 g l^{-1} and 1.13 g l^{-1}, respectively (Fig. 4c), and the maximum productivity of BDO was 0.67 g l^{-1} h^{-1} (Fig. 4d). These results show great promise for the scaling up of chemical production with biohybrids using wastewater.

We used LCA to compare BDO production by lab-scale wastewater-based biohybrids with current production from fossil-fuels and bacterial fermentation of sugars (Fig. 5a). To quantify the practical effects of biohybrid synthesis, a model used for the evaluation of industrial fermentation was modified and employed here to overcome

https://doi.org/10.1038/s41893-023-01233-2

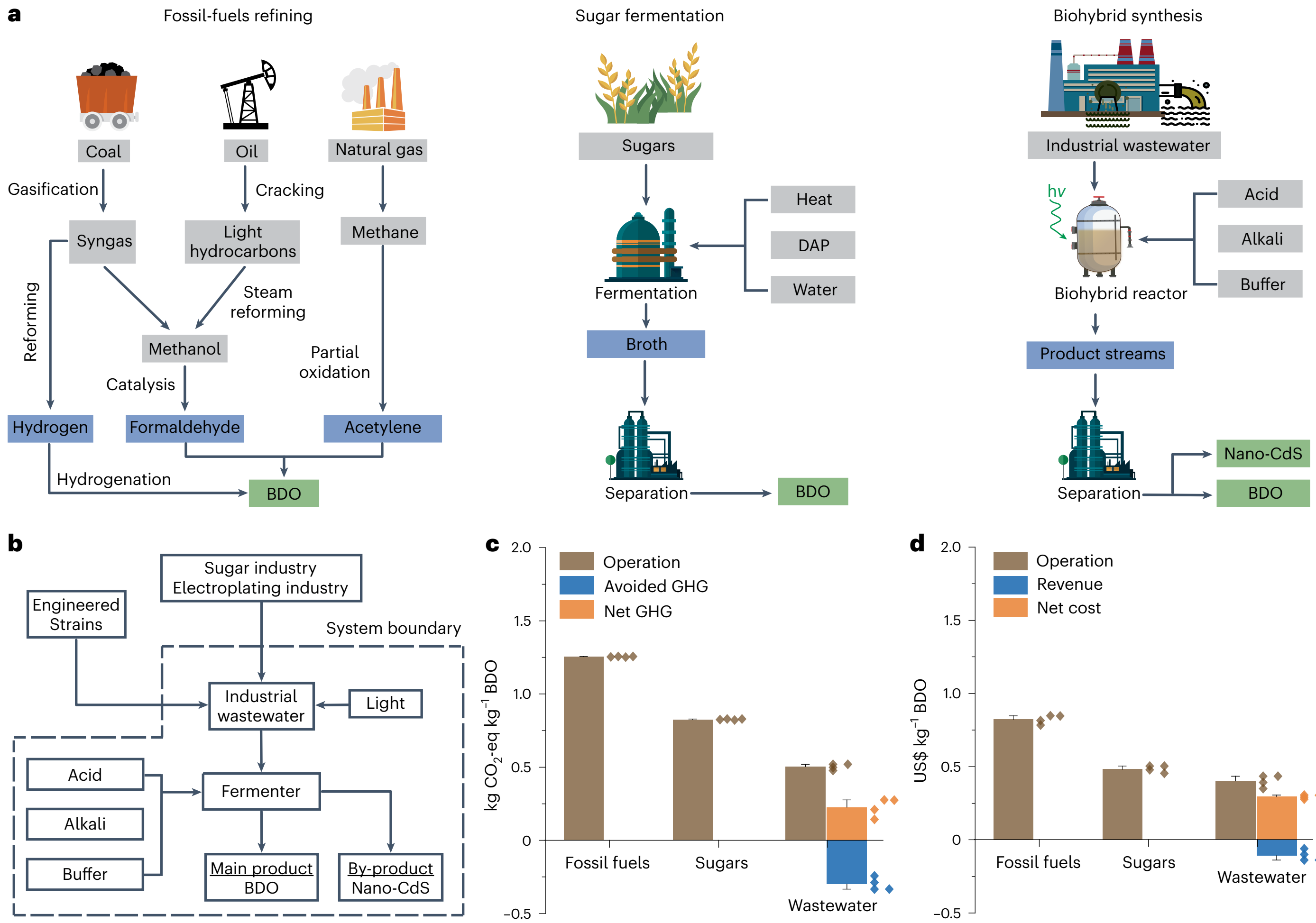

Fig. 5 | Life-cycle assessment. a, Comparison of current routes to BDO by fossil-fuels refining, sugar fermentation and solar-driven biohybrid synthesis from wastewater. DAP, diammoniumphosphate. **b**–**d**, System boundary of LCA for solar-driven biohybrid synthesis from wastewater, and comparison of GHG emissions (**c**) and economic cost (**d**) with current routes. Avoided treatment of industrial wastewater and by-products of nano-CdS offset partial GHG emissions and cost. Net GHG emission (orange) of BDO incorporates the positive emissions from operation (brown) of solar-driven biohybrid synthesis and avoided emissions (blue) from industrial wastewater treatment, net cost (orange) benefits from the revenues (blue) of avoided wastewater treatment and valuable by-products. Bar charts, error bars and data distribution ($n = 4$, the maximum, minimum, median and mean values were presented as the dots next to the charts.) were derived from 10,000 trials of Monte Carlo simulation with 10%–90% confidence interval.

the uncertainties in the lab-scale level (Fig. 5b). Both the GHG emission and cost of BDO production by biohybrids (0.50 ± 0.02 kg CO_2-eq kg^{-1} BDO, US\$$0.39 \pm 0.04$ kg^{-1} BDO) at the 10%-90% confidence interval are superior to those of fossil-fuels production (1.25 ± 0.002 kg CO_2-eq kg^{-1} BDO, US\$$0.82 \pm 0.03$ kg^{-1} BDO) and pure sugar fermentation (0.83 ± 0.003 kg CO_2-eq kg^{-1} BDO, US\$$0.48 \pm 0.02$ kg^{-1} BDO) (Fig. 5c,d). The lower GHG emission and cost are attributed to the utilization of wastewater as feedstock to partially reduce the requirement for wastewater treatment and recover CdS nanoparticles as revenues from integrating solar energy during biomanufacturing (Supplementary Table 6). The biohybrid system also exhibits the lowest environmental impacts in terms of resource consumption, terrestrial ecosystems and acidification, human health and so on due to its dual merits of both sustainable resource recovery and environmental remediation (Supplementary Fig. 12 and Table 7). It should be noted that several factors not considered in our model, such as sacrificial agents, different separation efficiencies of photo-induced electron-hole pairs and competition between complex organics and metal ions could affect the life-cycle impacts of BDO production by biohybrids. Further work is needed for a more accurate LCA of chemical production by the biohybrid route using wastewater.

Discussion

Semiconductor biohybrids integrate the best attributes of biological whole-cell catalysts and semiconducting nanomaterials, enabling non-photosynthetic industrial microbial cell factories to utilize solar energy for chemical production[7]. Despite recent progress showing higher efficiency in biomanufacturing, production of semiconductor biohybrids in large scale remains difficult[8,9]. To address this challenge, we developed a cost-competitive and environmentally friendly approach that is promising for sustainable and scalable production of semiconductor biohybrids towards solar-driven chemical production utilizing multiple pollutants in wastewater. Compared with fossil-fuels refining and sugar-based bacterial fermentation, the wastewater-derived biohybrid system shows lower carbon emission and production cost. The currently centralized management of different wastewater-emitting facilities in many countries will enable the use of various types of wastewater with stable compositions at the same location for the production of biohybrid systems[50]. We believe wastewater-based hybrid fermentation will provide an alternative for both sustainable biomanufacturing and environmental remediation.

In wastewater, the concurrent presence of varied organic compounds, heavy metal ions and sacrificial agents can compete with and influence BDO production in a CdS-biohybrid. Our initial findings suggest that the interplay among these pollutants can result in both positive and negative effects on production (Supplementary Figs. 10, 13 and 14). However, the challenges to the improvement of chemical productivity in wastewater, including variability in light penetration and electron sacrificial agents, competition among different pollutants, the complicated process of chemical separation and purification and so on, need to be overcome in future large-scale applications. In addition, understanding the mechanism of electron transfer occurring on the interface between semiconductor and bacterial cells is also necessary for future biohybrid modulation to achieve highly efficient solar-to-chemical production.

Methods

Industrial wastewater

Three kinds of organic wastewaters generated during production of biodiesel, sugar and corn starch, respectively, were obtained from factories in Harbin and Xingtai, China. These organic wastewaters have complex organic/inorganic compositions and are known to contain major organic wastes of crude glycerol, molasses and starch, respectively, which are considered as pollutants in water since their recycling by conventional physical/chemical approaches is uneconomical. We named these organic wastewaters as glycerol wastewater, molasses wastewater (composition in Supplementary Table 3) and starch wastewater, respectively. Electroplating wastewater (composition in Supplementary Table 5) was obtained from a metal electroplating factory in Shenzhen, China.

Bacterial culture media

(1) Rich culture medium: The LBv2 medium (per 1 l) contains 25 g LB powder, 11.9 g NaCl, 0.313 g KCl and 2.2 g $MgCl_2$ with corresponding antibiotics. All solidified media contain 1.5% (w/v) agar. (2) Well-defined minimum medium (MM): The modified M9 medium (per 1 l) contains 1 g NH_4Cl, 12.4 g NaCl, 10.99 g Tris-HCl, 0.34 g thiamine HCl, 10 ml 40% glycerol, 1 g casmino acid, 2 mM $MgSO_4$, 0.1 mM $CaSO_4$, 0.313 g KCl, 2.2 g $MgCl_2$, and pH was adjusted to 7.0 before use. (3) Wastewater medium: Wastewater medium was prepared by mixing electroplating wastewater and organic wastewater in a proportion and was amended with Cd^{2+} and salts (per 1 l) containing 5 g $(NH_4)_2SO_4$, 15 g NaCl, 1 g K_2HPO_4, 1 g KH_2PO_4, 0.25 g $MgSO_4$ and 0.01 g $CaCl_2$ in consideration of the tough condition of industrial wastewater with high salinity. The main components and properties of wastewater after pH adjustment are given in Supplementary Table 4. *V. natriegens* was routinely cultured using rich culture medium. The well-defined MM or wastewater medium was used for the construction of biohybrids and chemical production, respectively.

Engineering *V. natriegens*

The bacterial strains and plasmids are listed in Supplementary Table 8. Electroporation transformation was adapted from previously described protocol[51], with details provided in Supplementary Methods. For plasmids and strains construction, the DNA fragments containing the *cdsH* gene from *Treponema denticola*, and the mutant *cysE* gene with the promoter[24] were chemically synthesized by Genscript. The synthetic DNA fragments were cloned into the vector pUC-GW-Kan to generate plasmid pXG203. The plasmid pXG203 was introduced into *V. natriegens* VnDx, resulting in strain XG203. The BDO gene cluster containing its whole operon and the LysR-type transcriptional regulator from *Enterobacter cloacae* subsp. *dissolvens* SDM was amplified through PCR with the primer pairs RABC-overlap-F (5′-3′: gcataatgct taagtcttcctttcgggctttgttag) and RABC-overlap-R (5′-3′: tattgctcagcg gtggatataggcgccagcaac). The linearized pACYCduet-1 vector was amplified with the primer pairs pACYC-F (5′-3′: caccgctgagcaataactagc) and pACYC-R (5′-3′: acttaagcattatgcggccgc). The two fragments were assembled by Gibson assembly, resulting in the plasmid pACYC-RABC. The plasmid pACYC-RABC was introduced into *V. natriegens* XG203 to generate strain XG203A. The *mtrC* gene deletion was done by homologous recombination[52].

Quantifying gas production

H_2S gas was quantified using an IFU hydrogen sulfide Dräger tube (Dräger). A made-to-measure rubber stopper fitted to the Dräger tube was corked into 250 ml Erlenmeyer flasks containing 50 ml cultures[17]. To quantify gas production, strain XG203 or wild-type *V. natriegens* was cultured in well-defined MM at 37 °C for 72 h at an initial optical density $(OD)_{600}$ of ~0.6, and the numbers on the Dräger tube were recorded at specific timepoints. Strain XG203A was cultured in 100 ml Erlenmeyer flasks containing 20 ml wastewater medium with molasses wastewater as carbon substrate at an initial OD_{600} of ~1.0, and H_2S production was monitored under illumination (4.2 mW cm^{-2}). CO_2 gas was analysed by gas chromatography (GC) (Thermo Scientific TRACE 1310, Thermo Fisher).

Biohybrid construction and heavy metal removal

Strain XG203 was cultured in rich culture medium at 37 °C for ~3 h, and then 1% bacterial culture was transferred into a fresh rich culture medium and grown at 37 °C for another ~3 h. Cells were collected and resuspended in well-defined MM with separate addition of various metal ions ($CdCl_2$, $PbCl_2$, $CuSO_4$, $ZnCl_2$, Na_2SeO_3, $Bi(NO_3)_3{\cdot}5H_2O$, and $HgCl_2$) at an initial OD_{600} of ~0.6. The concentration of all metal ions was 0.1 mM, except for Hg^{2+} (0.01 mM). The supernatants were collected after culture at 37 °C for 24 h to measure the removal efficiency by ICP–MS (NexION 1000, PerkinElmer). The pellets were collected to analyse biohybrids and nanoparticles. Cd^{2+} removal by the wild-type *V. natriegens* was explored using the same conditions, and the pellets were collected to explore the interaction between bacterial cells and Cd^{2+}.

SEM

The collected pellets were fixed using 2.5% glutaraldehyde and stored at 4 °C overnight. The fixed pellets were then sequentially submerged in a series of ethanol (30%, 50%, 70%, 80%, 90% and 95%) for 15 min each and then in 100% ethanol for 20 min twice, ethanol:isoamyl acetate (v:v, 1:1) for 30 min and isoamyl acetate for 1 h. The samples were dried using a critical-point dryer (Leica EM CPD30) and imaged by SEM (HITACHI) with EDS after gold spraying.

Nanoparticles extraction

The collected pellets were resuspended in Tris-HCl (50 mM, pH 7.5) by sonication in an ice bath for 3 h using a probe sonicator (Scientz-IID) and then centrifuged at 13,000 × *g* for 1 h to collect the nanoparticles. The particles were dispersed with Li_2S/formamide solution (5 g l^{-1}) by sonication for 15 min and then didodecyldimethylammonium bromide (DDAB)/toluene (50 g l^{-1}) was added to the top of the obtained uniform solution with continuous stirring overnight. The DDAB-modified nanoparticles were collected from the top layer of the solution (oil layer), washed with acetone and ethanol three times to remove excess DDAB, centrifuged at 9,391 × *g* for 10 min and redispersed in toluene. The nanoparticles were analysed by transmission electron microscopy (TEM), X-ray powder diffraction and photoelectrochemical measurement.

Special aberration corrected TEM (AC-TEM)

To observe the morphology of semiconductor biohybrids, cross-sectional samples were prepared. The fixed pellets were centrifuged and washed with PBS (0.1 M, pH 7.4) three times, and then suspended and wrapped in 1% agarose solution before solidification. Agarose blocks were fixed with 1% osmium tetroxide in PBS (0.1 M, pH 7.4) for 2 h and then rinsed in PBS (0.1 M, pH 7.4) three times for 15 min each. For dehydration, the samples were exposed in a series of ethanol (30%, 50%, 70%, 80%, 90%, 95%, 100%, 100%) for 20 min and then submerged in acetone for 15 min twice. The samples were exposed in acetone/EMBed 812 (1:1) for 2–4 h, acetone/EMBed 812 (1:2) overnight, pure EMBed 812 for 5~8 h for resin penetration and embedding at 37 °C, inserted into embedding models poured with pure EMBed 812 at 37 °C overnight and then polymerized at 65 °C for 48 h in the oven. The resin blocks were cut to 60~80 nm thin using an ultra microtome (UC7, Leica) with diamond knife (Ultra 45°, Daitome), and fished out onto the copper grid of 200 meshes. The vaccum-dried copper grids with the cross-sectional semiconductor biohybrids and dispersed nanoparticles were observed using AC-TEM (JEM-ARM300F, JEOL). HAADF–STEM, EDS mapping and SAED were performed at 300 kV.

XPS

To distinguish the elemental composition of the wild-type *V. natriegens* with Cd^{2+} and the valence state of the element in semiconductor biohybrids, the freeze-dried pellets were analysed by XPS (Nexsa, Thermo Scientific) using Al Kα-ray at a work voltage of 15 kV using 1,486.6 eV energy, and the data were calibrated using C 1s at 284.80 eV.

Fourier transform infrared (FTIR) spectrometry

To analyse the change of functional groups in the wild-type *V. natriegens* after absorbing Cd^{2+}, the freeze-dried pellets were analysed by FTIR (Niolet iN10, Thermo Fisher) at the wavenumber of 400~4,000 cm^{-1}.

XRD

To determine the crystal structure of semiconductor nanoparticles, XRD patterns were detected using an XRD instrument (Areis, PANalytical) at 20~80°.

Photoelectrochemical analysis

UV–Vis (Thermo Fisher) was used to measure the direct bandgap. Electrochemical analysis was performed using the electrochemical workstation (INTERFACE 1010e, Gamry Instruments). The dispersed nanoparticles and semiconductor biohybrids were loaded on indium tin oxides (ITO) and carbon paper, respectively, to form a uniform 1 × 1 cm^2 film by drop casting and vaccum drying. The photoelectrochemical measurements were performed using a standard three-electrode configuration in electrolyte (0.5 M Na_2SO_4) and PBS buffer, respectively. Ag/AgCl (3 M NaCl) and platinum wire served as the reference and counter electrode, respectively. A 300 W Xe-arc lamp (Newport) equipped with a filter to block the infrared irradiation was employed as the solar simulator. The light intensity was calibrated to 1 sun illumination (100 mW cm^{-2}) by a light meter with optothermal detector (PM400, THORLABS). The current density was recorded under 0.5 V bias vs Ag/AgCl. The Mott–Schottky equation was used to clarify the conduction band of isolated nanoparticles at 1.0 kHz voltage.

Semiconductor biohybrid production from wastewater

To demonstrate the capability to utilize organics in wastewater, strain XG203 was cultured using wastewater-containing organics (5 g l^{-1}) as carbon source in well-defined MM with addition of $CdCl_2$ (0.1 mM). To clarify the capability to utilize various sources of wastewater, strain XG203 was cultured in well-defined MM with addition of $CdCl_2$ (0.01~0.2 mM), $PbCl_2$ (0.01~0.3 mM) or $HgCl_2$ (0.001~0.05 mM). To explore the capability to produce semiconductor biohybrids using wastewater, strain XG203 was cultured in wastewater medium with organics supplied by glycerol wastewater, molasses wastewater and starch wastewater. The culture conditions were all at 37 °C for 24 h, with an initial OD_{600} of ~0.6.

Preparing semiconductor biohybrids for BDO production

To prepare semiconductor biohybrids, strain XG203A was inoculated into rich culture medium to an OD_{600} of ~1.0 and then 1% was transferred into rich culture medium. Cell pellets were collected at an OD_{600} of ~1.0 and resuspended to an OD_{600} of ~0.6 in well-defined MM with addition of $CdCl_2$ (0.1 mM) or $PbCl_2$ (0.1 mM). The biohybrids were collected and cultured in well-defined MM with addition of glucose (5 g l^{-1}), cysteine (1 mM) and flavine mononucleotide sodium (5 μM) at 30 °C under dark or light conditions (4.2 mW cm^{-2}) for 24 h. The light intensity was calibrated using a light meter with optothermal detector (PM400, THORLABS). The supernatant was used to quantify BDO concentration, and the cell pellets were collected to quantify intracellular metabolites. The same condition was also used to culture pure bacterial system (without $CdCl_2$) for BDO production as a control. The light intensity was optimized at the range of 0~6.0 mW cm^{-2}, and the intracellular reactive oxygen species (ROS) of pure bacteria and biohybrids were detected using the ROS assay kit (Beyotime). To clarify the effects of coexisting pollutants in the wastewater on BDO production by this glucose-cysteine-based biohybrids, the same condition was also used for BDO production using glucose with other coexisting carbon sources (2 g l^{-1} maltose, starch, acetate or lactate) under illumination (4.2 mW cm^{-2}), or cysteine with coexisting carboxylic acid (0.1%~1% acetic acid or lactic acid) and alcohols (1% methanol, 0.1%~1% ethanol or 1% ethylene glycol). In addition, bacterial cultures were collected to construct biohybrids using the multiple coexisting heavy metals (final concentration of 0.1 mM Cd^{2+}, 0.1 mM Pb^{2+}, 0.05 mM Zn^{2+} and 0.05 mM Cu^{2+}) at an initial OD_{600} of ~1.0. The semiconductor biohybrid complex was collected to measure BDO production. To explore the role of redox proteins on electron transfer at the interface between semiconductors and bacterial cells, the mutant XG203A-Δ*mtrC*-CdS hybrid was constructed to measure BDO production using the above-mentioned method.

Quantifying metabolites in semiconductor biohybrids

We quantified intracellular metabolites using a previously reported extraction method for intracellular metabolites[53]. Briefly, cell pellets were collected by centrifugation at 8,000 × *g* for 5 min at 4 °C and resuspended immediately in 2 ml of methanol/water (80:20, v/v) pre-cooled at −80 °C. The samples were centrifuged at 14,000 × *g* for 10 min at 4 °C after incubation at −20 °C for 20 min. The supernatant was collected to quantify metabolites using LC–MS/MS (SCIEX Triple Quad 5000+ QTRAP Ready, AB SCIEX) and Q Exactive hybrid quadrupole–orbitrap mass spectrometer (Thermo Fisher) based on SCIEX OS-MQ 2.0, Exactive Series Tune 2.8 (Thermo), Analyst 1.7, Thermo Scientific Xcalibur 4.2.47 and Thermo Compound Discoverer 2.0.

Quantifying BDO, acetoin, glucose and cysteine

To determine BDO and acetoin concentration, bacterial cultures were centrifuged at 21,130 × *g* for 10 min and the supernatant was mixed with the isometric ethyl acetate with ultrasonication for 30 min and centrifugation for 10 min. Supernatant was filtered using nylon membrane (0.22 μm) and then determined using GC. The GC system (Agilent 8890, Agilent) was equipped with a DB-WAX capillary column (30 m × 0.53 mm × 1 μm) and a flame ionization detector. Hydrogen gas was used as the carrier gas. The injector and detector temperatures were maintained at 250 °C, and the oven temperature was 80 °C. The injection volume was 1 μl. Glucose and cysteine content were determined using glucose assay reagent (Beyotime) and cysteine content assay kit (Sangon Biotech), respectively.

Solar-driven BDO production by biohybrids in wastewater

To demonstrate the capability of semiconductor biohybrids for *in-situ* BDO production using wastewater, *V. natriegens* XG203A was inoculated into rich culture medium and cultured at 37 °C until an OD_{600} of ~1.0 and then 1% was transferred into fresh rich culture medium. The bacterial cells were collected at an OD_{600} of ~0.6, then resuspended and cultured using molasses wastewater (containing 4.68 g l^{-1} sugar) amended with salts (refer to wastewater medium) at 37 °C until an OD_{600} of ~1.0. Cell pellets were collected and cultured using wastewater medium with organics (4.10 g l^{-1} sugar) supplied by molasses wastewater at 37 °C for 1 h under dark and light conditions (4.2 mW cm^{-2}) at an initial bacterial OD_{600} of ~1.0. Cysteine (1 mM) and flavine mononucleotide sodium (5 μM) were added to the cultures. The pure bacterial system was cultured in molasses wastewater amended with salts (refer to wastewater medium) for BDO production using the same condition as the control. The supernatant was used to measure the concentration of BDO, acetoin and total sugar (anthrone-sulfuric acid method). To explore the impact of molasses concentration on the efficiency of biohybrids, *V. natriegens* XG203A was cultured in wastewater medium with organics supplied by different concentrations of molasses wastewater (from 3 to 48 g l^{-1}) at 37 °C for 24 h under light condition (4.2 mW cm^{-2}) at an initial bacterial OD_{600} of ~1.0. To demonstrate the generated semiconductor biohybrids and nanoparticles using wastewater with organics supplied by molasses wastewater, the pellets were collected for analysis of photoelectrochemical properties. In addition, the redox potential of reaction systems was determined by the oxidation–reduction potential composite electrodes (LEICI), and the generated gas composition of reaction systems was analysed using the Dräger tube and GC.

Scalable BDO production by wastewater-derived biohybrids

To scale up *in-situ* production of semiconductor biohybrids and BDO, *V. natriegens* XG203A was cultured using wastewater medium in a 5-l fermenter (Biostat A, Sartorius Stedim). Briefly, when the OD_{600} of XG203A cultured in rich culture medium reached ~1.0, the bacterial cultures were transferred into 4 l of molasses wastewater (containing 19.2 g sugar) amended with salts (refer to wastewater medium) by a 2% dilution. When OD_{600} reached ~1.0, the concentrated cultures were transferred into a 5-l fermenter containing 3 l of wastewater medium with organics supplied by molasses wastewater (containing 52.2 g sugar) under an illumination of 6 mW cm^{-2}. The parameters of the fermenter were set at 37 °C, pH 7.0, 600 r min^{-1}, and an air flow of 500 ccm. The samples were collected at specific time intervals to detect BDO, acetoin and total sugar.

LCA

LCA was conducted to analyse GHG emissions, economic cost and other comprehensive environmental impacts in terms of resource consumption, terrestrial ecosystems and acidification, human health and so on, with the scope of cradle-to-gate excluding utilities construction and end-of-life disposal[54,55]. Life-cycle inventory and emission factors in the production of 1 kg BDO using the conventional routes of fossil-fuels refining and biofermentation of pure sugars were calculated using the Ecoinvent database and models from the Argonne National Laboratory[54,56]. A modified industrial model of biochemical fermentation was adopted here to comprehensively evaluate the environmental and economic impacts of BDO production with less uncertainties according to the lab data of solar-driven biohybrid synthesis using wastewater. Conventional treatments of industrial wastewater consume chemicals and energy with auxiliary GHG emissions and investment. LCA was used to analyse the potential offset of GHG emission and economic cost by biohybrid synthesis, wherein wastewater treatment is avoided and another valuable by-product (nano-CdS) is produced. Life-cycle inventory and parameters for the detailed calculations are provided in Supplementary Tables 6, 7 and 9–15, including consumption of materials and energy for BDO production and separation, as well as conventional wastewater treatments. IPCC-2021-GWP100 (ref. 57) was conducted to quantify the GHG emission. An extended life-cycle economic evaluation based on similar goal and scope as LCA was used to calculate the economic burdens of the whole life-cycle process[58,59].

GHG emission and other environmental impacts such as terrestrial acidification or human toxicity were calculated on the basis of the following equation:

$$\mathrm{EI}_i = \sum_{j=1}^{n} (\mathrm{CA}_j \times \mathrm{EF}_j) \quad (1)$$

where EI_i represents the environmental impacts (EI) of process *i*, which includes production of 1 kg BDO by fossil-fuels refining, sugar fermentation and biohybrid synthesis using wastewater. CA_j indicates the consumption amount (CA) of *j* (for example, materials, chemicals, energy) for BDO production. EF_j refers to the environmental factor (EF) of *j* consumed for BDO production, which was obtained from the assessment using IPCC-2021-GWP100 and ReCiPe-2016-Midpoint-(H)[57].

Reporting summary

Further information on research design is available in the Nature Portfolio Reporting Summary linked to this article.

Data availability

All data presented in this manuscript are available in the paper and its Supplementary Information. Figures 1–5 and Supplementary Figs. 1–14, 16, 18 and 20 are available on Figshare at https://doi.org/10.6084/m9.figshare.24115851. Source data are provided with this paper.

References

1. Scown, C. D. & Keasling, J. D. Sustainable manufacturing with synthetic biology. *Nat. Biotechnol.* **40**, 304–307 (2022).
2. Liew, F. E. et al. Carbon-negative production of acetone and isopropanol by gas fermentation at industrial pilot scale. *Nat. Biotechnol.* **40**, 335–344 (2022).
3. Liu, Y. Z. et al. Biofuels for a sustainable future. *Cell* **184**, 1636–1647 (2021).
4. Jones, S. W. et al. CO_2 fixation by anaerobic non-photosynthetic mixotrophy for improved carbon conversion. *Nat. Commun.* **7**, 12800 (2016).
5. Sakimoto, K. K., Wong, A. B. & Yang, P. D. Self-photosensitization of nonphotosynthetic bacteria for solar-to-chemical production. *Science* **351**, 74–77 (2016).
6. Guo, J. L. et al. Light-driven fine chemical production in yeast biohybrids. *Science* **362**, 813–816 (2018).
7. Cestellos-Blanco, S., Zhang, H., Kim, J. M., Shen, Y. X. & Yang, P. D. Photosynthetic semiconductor biohybrids for solar-driven biocatalysis. *Nat. Catal.* **3**, 245–255 (2020).
8. Kornienko, N., Zhang, J. Z., Sakimoto, K. K., Yang, P. D. & Reisner, E. Interfacing nature's catalytic machinery with synthetic materials for semi-artificial photosynthesis. *Nat. Nanotechnol.* **13**, 890–899 (2018).
9. Cestellos-Blanco, S., Kim, J. M., Watanabe, N. G., Chan, R. R. & Yang, P. D. Molecular insights and future frontiers in cell photosensitization for solar-driven CO_2 conversion. *iScience* **24**, 102952 (2021).
10. Kang, S. H., Bozhilov, K. N., Myung, N. V., Mulchandani, A. & Chen, W. Microbial synthesis of CdS nanocrystals in genetically engineered *E. coli*. *Angew. Chem. Int. Ed.* **47**, 5186–5189 (2008).
11. Kornienko, N. et al. Spectroscopic elucidation of energy transfer in hybrid inorganic-biological organisms for solar-to-chemical production. *Proc. Natl Acad. Sci. USA* **113**, 11750–11755 (2016).
12. Wang, B., Jiang, Z. F., Yu, J. C., Wang, J. F. & Wong, P. K. Enhanced CO_2 reduction and valuable C_{2+} chemical production by a CdS-photosynthetic hybrid system. *Nanoscale* **11**, 9296–9301 (2019).
13. Yan, N., Zhou, K., Tong, Y. W., Leong, D. T. & Dickieson, M. P. Pathways to food from CO_2 via 'green chemical farming'. *Nat. Sustain.* **5**, 907–909 (2022).
14. Li, W. W., Yu, H. Q. & Rittmann, B. E. Chemistry: reuse water pollutants. *Nature* **528**, 29–31 (2015).
15. Sullivan, K. P. et al. Mixed plastics waste valorization through tandem chemical oxidation and biological funneling. *Science* **378**, 207–211 (2022).
16. Atelge, M. R. et al. Biogas production from organic waste: recent progress and perspectives. *Waste Biomass Valor.* **11**, 1019–1040 (2020).

17. Sun, G. L., Reynolds, E. E. & Belcher, A. M. Using yeast to sustainably remediate and extract heavy metals from waste waters. *Nat. Sustain.* **3**, 303–311 (2020).
18. Oh, S. & Logan, B. E. Hydrogen and electricity production from a food processing wastewater using fermentation and microbial fuel cell technologies. *Water Res.* **39**, 4673–4682 (2005).
19. Nam, J. Y., Yates, M. D., Zaybak, Z. & Logan, B. E. Examination of protein degradation in continuous flow, microbial electrolysis cells treating fermentation wastewater. *Bioresour. Technol.* **171**, 182–186 (2014).
20. Kieu, H. T., Muller, E. & Horn, H. Heavy metal removal in anaerobic semi-continuous stirred tank reactors by a consortium of sulfate-reducing bacteria. *Water Res.* **45**, 3863–3870 (2011).
21. Javanbakht, V., Alavi, S. A. & Zilouei, H. Mechanisms of heavy metal removal using microorganisms as biosorbent. *Water Sci. Technol.* **69**, 1775–1787 (2014).
22. De Vrieze, J., Coma, M., Debeuckelaere, M., Van der Meeren, P. & Rabaey, K. High salinity in molasses wastewaters shifts anaerobic digestion to carboxylate production. *Water Res.* **98**, 293–301 (2016).
23. Jassby, D., Cath, T. Y. & Buisson, H. The role of nanotechnology in industrial water treatment. *Nat. Nanotechnol.* **13**, 670–672 (2018).
24. Wang, C. L., Maratukulam, P. D., Lum, A. M., Clark, D. S. & Keasling, J. D. Metabolic engineering of an aerobic sulfate reduction pathway and its application to precipitation of cadmium on the cell surface. *Appl. Environ. Microbiol.* **66**, 4497–4502 (2000).
25. Zeng, Q., Hao, T. W., Mackey, H. R., van Loosdrecht, M. C. M. & Chen, G. H. Recent advances in dissimilatory sulfate reduction: from metabolic study to application. *Water Res.* **150**, 162–181 (2019).
26. Xu, J. Q., Yang, S. & Yang, L. R. *Vibrio natriegens* as a host for rapid biotechnology. *Trends Biotechnol.* **40**, 381–384 (2022).
27. Tait, S., Clarke, W. P., Keller, J. & Batstone, D. J. Removal of sulfate from high-strength wastewater by crystallisation. *Water Res.* **43**, 762–772 (2009).
28. Riahi, S. & Rowley, C. N. Why can hydrogen sulfide permeate cell membranes? *J. Am. Chem. Soc.* **136**, 15111–15113 (2014).
29. Sakpirom, J., Kantachote, D., Siripattanakul-Ratpukdi, S., McEvoy, J. & Khan, E. Simultaneous bioprecipitation of cadmium to cadmium sulfide nanoparticles and nitrogen fixation by *Rhodopseudomonas palustris* TN110. *Chemosphere* **223**, 455–464 (2019).
30. Wang, B. et al. Biohybrid photoheterotrophic metabolism for significant enhancement of biological nitrogen fixation in pure microbial cultures. *Energy Environ. Sci.* **12**, 2185–2191 (2019).
31. Xu, R. et al. New double network hydrogel adsorbent: highly efficient removal of Cd(II) and Mn(II) ions in aqueous solution. *Chem. Eng. J.* **275**, 179–188 (2015).
32. Luo, X. B., Xi, Y., Yu, H. Y., Yin, X. C. & Luo, S. L. Capturing cadmium(II) ion from wastewater containing solid particles and floccules using ion-imprinted polymers with broom effect. *Ind. Eng. Chem. Res.* **56**, 2350–2358 (2017).
33. Liu, T. Y., Yang, X., Wang, Z. L. & Yan, X. X. Enhanced chitosan beads-supported Fe^0-nanoparticles for removal of heavy metals from electroplating wastewater in permeable reactive barriers. *Water Res.* **47**, 6691–6700 (2013).
34. Suzuki, Y., Kametani, T. & Maruyama, T. Removal of heavy metals from aqueous solution by nonliving *Ulva* seaweed as biosorbent. *Water Res.* **39**, 1803–1808 (2005).
35. Goncalves, M. M. M., da Costa, A. C. A., Leite, S. G. F. & Sant'Anna, G. L. Jr Heavy metal removal from synthetic waste-waters in an anaerobic bioreactor using stillage from ethanol distilleries as a carbon source. *Chemosphere* **69**, 1815–1820 (2007).
36. D'Angelo, S. C., Dall'Ara, A., Mondelli, C., Pérez-Ramírez, J. & Papadokonstantakis, S. Techno-economic analysis of a glycerol biorefinery. *ACS Sustain. Chem. Eng.* **6**, 16563–16572 (2018).
37. Quispe, C. A. G., Coronado, C. J. R. & Carvalho, J. A. Jr. Glycerol: production, consumption, prices, characterization and new trends in combustion. *Renew. Sustain. Energy Rev.* **27**, 475–493 (2013).
38. Ye, J. et al. Light-driven carbon dioxide reduction to methane by *Methanosarcina barkeri*-CdS biohybrid. *Appl. Catal. B* **257**, 117916 (2019).
39. Ji, X. J., Huang, H. & Ouyang, P. K. Microbial 2,3-butanediol production: a state-of-the-art review. *Biotechnol. Adv.* **29**, 351–364 (2011).
40. Celinska, E. & Grajek, W. Biotechnological production of 2,3-butanediol-current state and prospects. *Biotechnol. Adv.* **27**, 715–725 (2009).
41. Xu, Y. Q. et al. Systematic metabolic engineering of *Escherichia coli* for high-yield production of fuel bio-chemical 2,3-butanediol. *Metab. Eng.* **23**, 22–33 (2014).
42. Zhang, H. et al. Bacteria photosensitized by intracellular gold nanoclusters for solar fuel production. *Nat. Nanotechnol.* **13**, 900–905 (2018).
43. Wei, W. et al. A surface-display biohybrid approach to light-driven hydrogen production in air. *Sci. Adv.* **4**, eaap9253 (2018).
44. Ding, Y. C. et al. Nanorg microbial factories: light-driven renewable biochemical synthesis using quantum dot-bacteria nanobiohybrids. *J. Am. Chem. Soc.* **141**, 10272–10282 (2019).
45. Wang, M., Chen, B. Q., Fang, Y. M. & Tan, T. W. Cofactor engineering for more efficient production of chemicals and biofuels. *Biotechnol. Adv.* **35**, 1032–1039 (2017).
46. Zhang, R. T. et al. Proteomic and metabolic elucidation of solar-powered biomanufacturing by bio-abiotic hybrid system. *Chem* **6**, 234–249 (2020).
47. Bo, T. T. et al. Photocatalytic H_2 evolution on CdS modified with partially crystallized MoS_2 under visible light irradiation. *Chem. Phys. Lett.* **746**, 137305 (2020).
48. Jin, S. et al. Acetogenic bacteria utilize light-driven electrons as an energy source for autotrophic growth. *Proc. Natl. Acad. Sci. USA* **118**, e2020552118 (2021).
49. Guan, X. et al. Maximizing light-driven CO_2 and N_2 fixation efficiency in quantum dot-bacteria hybrids. *Nat. Catal.* **5**, 1019–1029 (2022).
50. Hu, W. Q., Tian, J. P., Zang, N., Gao, Y. & Chen, L. J. Study of the development and performance of centralized wastewater treatment plants in Chinese industrial parks. *J. Clean. Prod.* **214**, 939–951 (2019).
51. Weinstock, M. T., Hesek, E. D., Wilson, C. M. & Gibson, D. G. *Vibrio natriegens* as a fast-growing host for molecular biology. *Nat. Methods* **13**, 849–851 (2016).
52. Zhang, Y. et al. Systems metabolic engineering of *Vibrio natriegens* for the production of 1,3-propanediol. *Metab. Eng.* **65**, 52–65 (2021).
53. Gao, X. et al. Engineering the methylerythritol phosphate pathway in cyanobacteria for photosynthetic isoprene production from CO_2. *Energy Environ. Sci.* **9**, 1400–1411 (2016).
54. Wernet, G. et al. The ecoinvent database version 3 (part I): overview and methodology. *Int. J. Life Cycle Assess.* **21**, 1218–1230 (2016).
55. *Lifecycle Analysis of Greenhouse Gas Emissions Under the Renewable Fuel Standard* (US EPA, 2021).
56. Dunn, J. B. et al. *Life-cycle Analysis of Bioproducts and their Conventional Counterparts in GREET* Technical Report (US Department of Energy, 2015).
57. *2019 Refinement to the 2006 IPCC Guidelines for National Greenhouse Gas Inventories* (IPCC, 2019).

58. Jiang, H., Jin, Q., Cheng, P. P., Hua, M. & Ye, Z. How are typical urban sewage treatment technologies going in China: from the perspective of life cycle environmental and economic coupled assessment. *Environ. Sci. Pollut. Res.* **28**, 45109–45120 (2021).
59. Pi, S. S. et al. Solar-driven waste-to-chemical conversion by wastewater-derived semiconductor biohybrids. *Figshare* https://doi.org/10.6084/m9.figshare.24115851 (2023).

Acknowledgements

We thank C. Zhong for valuable suggestions and discussion of this work and the Shenzhen Infrastructure for Synthetic Biology for instrument support and technical assistance. This work was supported by the National Natural Science Foundation of China (Grant No. 32230060, C.Y. and X.G.; Grant No. 22176046, L.L.; Grant No. 32171426, X.G.; Grant No. 52200090, S.P.), Shenzhen Science and Technology Program (Grant No. GXWD20220811173949005, KQTD20190929172630447 and JCYJ20210324124209025, L.L.; Grant No. JCYJ20220818101804010, RCYX20221008092901004, X.G.), the National Key R&D Program of China (Grant No. 2021YFA0910800, X.G.), State Key Laboratory of Urban Water Resource and Environment (Harbin Institute of Technology) (Grant No. 2021TS13, L.L.) and the Natural Science Foundation of Guangdong Province (Grant No. 2022A1515012016, L.L.).

Author contributions

X.G., L.L., Y.L. and C.Y. supervised the research; X.G. and L.L. designed the experiments; S.P., W.Y. and W.F. contributed to the biohybrid production, and the structural and chemical characterizations; W. Cheng and S.P. performed the metabolic experiment, with the results verified by X.G.; S.P., R.Y. and W.Y. contributed to the wastewater-relevant experiments and fermenter data; L.C., Z.L., R.Y. and W. Chao performed the photoelectrochemical analysis; W. Chao, N.R., X.G. and L.L. contributed to the LCA data; S.P., X.G., Y.L., L.L., W.Y. and W. Chao wrote the manuscript and received comments from all the other authors.

Competing interests

L.L., X.G., R.Y., S.P. and W.Y. are co-inventors on filed China patents CN202310145122.9 and CN202210318999.9 related to the production of semiconductor nanoparticles and biohybrids directly from wastewater by engineered strains that incorporate discoveries included in this manuscript. The remaining authors declare no competing interests.

Additional information

Supplementary information The online version contains supplementary material available at https://doi.org/10.1038/s41893-023-01233-2.

Correspondence and requests for materials should be addressed to Lu Lu or Xiang Gao.

Peer review information *Nature Sustainability* thanks Shu Wang and the other, anonymous, reviewer(s) for their contribution to the peer review of this work.

[1]State Key Laboratory of Urban Water Resource and Environment, School of Civil and Environmental Engineering, Harbin Institute of Technology, Shenzhen, China. [2]Center for Materials Synthetic Biology, CAS Key Laboratory of Quantitative Engineering Biology of CAS, Shenzhen Institute of Synthetic Biology, Shenzhen Institutes of Advanced Technology, Chinese Academy of Science, Shenzhen, China. [3]Materdicine Lab, School of Life Sciences, Shanghai University, Shanghai, China. [4]CAS-Key Laboratory of Synthetic Biology, CAS Center for Excellence in Molecular Plant Sciences, Institute of Plant Physiology and Ecology, Chinese Academy of Sciences, Shanghai, China. [5]Department of Chemical and Biomolecular Engineering, National University of Singapore, Singapore, Singapore. [6]These authors contributed equally: Shanshan Pi, Wenjun Yang, Wei Feng. ✉e-mail: lulu@hit.edu.cn; gaoxiang@siat.ac.cn

nature portfolio

Corresponding author(s): Xiang Gao; Lu Lu

Last updated by author(s): Sep 8, 2023

Reporting Summary

Nature Portfolio wishes to improve the reproducibility of the work that we publish. This form provides structure for consistency and transparency in reporting. For further information on Nature Portfolio policies, see our Editorial Policies and the Editorial Policy Checklist.

Statistics

For all statistical analyses, confirm that the following items are present in the figure legend, table legend, main text, or Methods section.

n/a	Confirmed	
☐	☒	The exact sample size (*n*) for each experimental group/condition, given as a discrete number and unit of measurement
☐	☒	A statement on whether measurements were taken from distinct samples or whether the same sample was measured repeatedly
☐	☒	The statistical test(s) used AND whether they are one- or two-sided *Only common tests should be described solely by name; describe more complex techniques in the Methods section.*
☒	☐	A description of all covariates tested
☒	☐	A description of any assumptions or corrections, such as tests of normality and adjustment for multiple comparisons
☐	☒	A full description of the statistical parameters including central tendency (e.g. means) or other basic estimates (e.g. regression coefficient) AND variation (e.g. standard deviation) or associated estimates of uncertainty (e.g. confidence intervals)
☒	☐	For null hypothesis testing, the test statistic (e.g. *F*, *t*, *r*) with confidence intervals, effect sizes, degrees of freedom and *P* value noted *Give P values as exact values whenever suitable.*
☒	☐	For Bayesian analysis, information on the choice of priors and Markov chain Monte Carlo settings
☒	☐	For hierarchical and complex designs, identification of the appropriate level for tests and full reporting of outcomes
☒	☐	Estimates of effect sizes (e.g. Cohen's *d*, Pearson's *r*), indicating how they were calculated

Our web collection on statistics for biologists contains articles on many of the points above.

Software and code

Policy information about availability of computer code

Data collection	Intracellular metabolites data were collected using SCIEX OS-MQ 2.0 and Exactive Series Tune 2.8 (Thermo).
Data analysis	Intracellular metabolites data were analyzed using Analyst 1.7, Thermo Scientific Xcalibur 4.2.47, and Thermo Compound Discoverer 2.0.

For manuscripts utilizing custom algorithms or software that are central to the research but not yet described in published literature, software must be made available to editors and reviewers. We strongly encourage code deposition in a community repository (e.g. GitHub). See the Nature Portfolio guidelines for submitting code & software for further information.

Data

Policy information about availability of data

All manuscripts must include a data availability statement. This statement should provide the following information, where applicable:

- Accession codes, unique identifiers, or web links for publicly available datasets
- A description of any restrictions on data availability
- For clinical datasets or third party data, please ensure that the statement adheres to our policy

Data Availability Statement: All data presented in this manuscript are available in the paper and Supplementary Information. Figure 1-5 and Supplementary Figure 1-14, 16, 18, and 20 are available on Figshare: https://doi.org/10.6084/m9.figshare.24115851.

March 2021

Human research participants

Policy information about studies involving human research participants and Sex and Gender in Research.

Reporting on sex and gender	NA
Population characteristics	NA
Recruitment	NA
Ethics oversight	NA

Note that full information on the approval of the study protocol must also be provided in the manuscript.

Field-specific reporting

Please select the one below that is the best fit for your research. If you are not sure, read the appropriate sections before making your selection.

☒ Life sciences ☐ Behavioural & social sciences ☐ Ecological, evolutionary & environmental sciences

For a reference copy of the document with all sections, see nature.com/documents/nr-reporting-summary-flat.pdf

Life sciences study design

All studies must disclose on these points even when the disclosure is negative.

Sample size	Sample size was determined based on extensive laboratory experience and literature in the field, such as the reference DOI: 10.1126/science.aat9777
Data exclusions	No data excluded for statistical analyses. Representative images were shown in the manuscripts; similar results from experimental repeats were not shown.
Replication	The number of biological replicates we aimed for was at least three with technical replicates in each group. All the experiments were performed independently and reliably reproduced weekly. Fermenter data at different time intervals were collected from one batch, and all attempts at replication were successful. Representative results in one batch were provided in the manuscripts; similar results from experimental repeats were not shown.
Randomization	Experimental groups were formed based on what was being tested with random sections. The same type of material and bacterial cells were used for all experiments.
Blinding	Experiments were blinded during imaging, metabolites measuring, and the investigators were blinded to group allocation. All data were analyzed by multiple authors and reviewed by the corresponding authors.

Reporting for specific materials, systems and methods

We require information from authors about some types of materials, experimental systems and methods used in many studies. Here, indicate whether each material, system or method listed is relevant to your study. If you are not sure if a list item applies to your research, read the appropriate section before selecting a response.

Materials & experimental systems

n/a	Involved in the study	
☒	☐	Antibodies
☒	☐	Eukaryotic cell lines
☒	☐	Palaeontology and archaeology
☒	☐	Animals and other organisms
☒	☐	Clinical data
☒	☐	Dual use research of concern

Methods

n/a	Involved in the study	
☒	☐	ChIP-seq
☒	☐	Flow cytometry
☒	☐	MRI-based neuroimaging